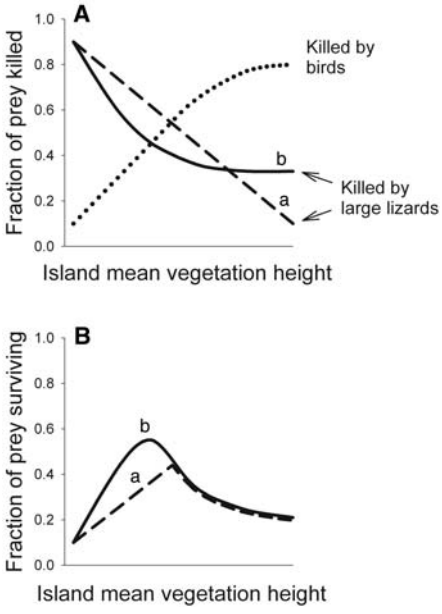

Fig. 3. (**A**) Hypothetical mortality curves as a function of vegetation height. The fraction of prey killed by the large introduced lizard predator decreases with vegetation height, either linearly (a) or asymptotically (b). The fraction of prey killed by natural predators such as itinerant birds increases with vegetation height, with a small asymptotic portion at the end. (**B**) Predicted survival curves as a function of vegetation height. These curves consist of two segments, the first of which is the complement (1 – fraction killed) of the large lizard predator curve to the left of the intersection, and the second is the complement of the itinerant bird predator curve to the right of the intersection.

predation by the large lizard is assumed to decline monotonically with vegetation height, either linearly (curve A) or asymptotically (curve B). The actual number killed by both predators is then the number killed by the introduced large lizard or the number killed by itinerant birds on the control island, whichever is larger. The resulting survival curves for introduction islands are depicted in Fig. 3B, which should be compared with the actual curves of Fig. 2. Although consistent with the data and hypothesized mechanisms involving itinerant birds, definitive evaluation awaits further investigation.

By using an archipelago of small islands as a laboratory for both comparative study and manipulative experiment, we showed a notable natural relation of survival rate to island characteristics—especially vegetation height—and the ability of an introduced predator to transform that relation. Implications of this study extend beyond islands: Vegetation structure over much of Earth's surface is being precisely characterized, in part to understand how species populations respond to anthropogenic changes in land use or in climate (*24*–*26*). However, information beyond vegetation structure may be crucial. Thus, in our study, survival is unrelated to vegetation height if data from all 12 islands are considered together (r = –0.23, –0.24), yet knowing which islands have the introduced predator makes the latter a good predictor of survival rates.

References and Notes

1. R. H. MacArthur, E. O. Wilson, *The Theory of Island Biogeography* (Princeton Univ. Press, Princeton, NJ, 1967).
2. J. M. Diamond, E. Mayr, *Proc. Natl. Acad. Sci. U.S.A.* **73**, 262 (1976).
3. M. L. Rosenzweig, *Species Diversity in Space and Time* (Cambridge Univ. Press, Cambridge, UK, 1995).
4. M. V. Lomolino, B. R. Riddle, J. H. Brown, *Biogeography* (Sinauer, Sunderland, MA, 2005).
5. R. E. Ricklefs, E. Bermingham, *Am. Nat.* **163**, 227 (2004).
6. R. D. Holt, in *Food Webs: Integration of Patterns and Dynamics*, G. A. Polis, K. O. Winemiller, Eds. (Chapman and Hall, New York, 1966), pp. 313–323.
7. A. Schoener, in *Analytical Biogeography*, A. A. Myers, P. S. Giller, Eds. (Chapman and Hall, London, 1988), pp. 483–512.
8. T. W. Schoener, A. Schoener, *J. Anim. Ecol.* **52**, 237 (1983).
9. Materials and methods are available as supporting material on *Science* Online.
10. J. B. Losos, T. W. Schoener, D. A. Spiller, *Nature* **432**, 505 (2004).
11. T. E. Philippi, in *Design and Analysis of Ecological Experiments*, S. M. Scheiner, J. Gurevich, Eds. (Chapman and Hall, New York, 1993), pp. 183–210.
12. T. W. Schoener, A. Schoener, *Nature* **302**, 332 (1983).
13. E. L. Charnov, *Theor. Pop. Biol.* **9**, 129 (1976).
14. D. W. Stephens, J. R. Krebs, *Foraging Theory* (Princeton Univ. Press, Princeton, NJ, 1986).
15. Deleterious effects increasing with density that are purely intraspecific are also possible. For the subject *A. sagrei*, it is unlikely that such effects—intraspecific competition for food and consequences of aggressive interactions—would by themselves result in mortality, because the lizards marked for this study were relatively large.
16. Moreover, *L. carinatus* is thermophilic, depending on sufficient sunlight for its activity during cooler times of the year. Islands having taller vegetation on average have less sunlight striking the ground, which is where *L. carinatus* mostly forage. Hence, their average predation rate should be lower on such islands.
17. J. E. Losey, R. F. Denno, *Ecology* **79**, 2143 (1999).
18. S. L. Lima, L. M. Dill, *Can. J. Zool.* **68**, 619 (1990).
19. A. Sih, G. Englund, D. Wooster, *Trends Ecol. Evol.* **13**, 350 (1998).
20. *L. carinatus*, the introduced predator, feeds on prey palatable to large birds other than small lizards, specifically large arthropods (*27*).
21. E. D. Brodie III, *Anim. Behav.* **45**, 851 (1993).
22. A. M. Castilla, A. Labra, *Acta Oecol.* **19**, 107 (1998).
23. J. S. Brown, *Behav. Ecol. Sociobiol.* **22**, 37 (1988).
24. A. T. Peterson, R. D. Holt, *Ecol. Lett.* **6**, 774 (2003).
25. K. Oberhauser, A. T. Peterson, *Proc. Natl. Acad. Sci. U.S.A.* **100**, 14063 (2003).
26. G. S. Olson *et al.*, *J. Wildl. Manage.* **68**, 1039 (2004).
27. T. W. Schoener, J. B. Slade, C. H. Stinson, *Oecologia* **53**, 160 (1982).

28. We thank J. Chase and reviewers for helpful comments, and the NSF and National Geographic Society for support.

Supporting Online Material

www.sciencemag.org/cgi/content/full/310/5755/1807/DC1
Materials and Methods
SOM Text
References

14 September 2005; accepted 9 November 2005
10.1126/science.1120165

Long-Term Modulation of Electrical Synapses in the Mammalian Thalamus

Carole E. Landisman[1,2]* and Barry W. Connors[1]

Electrical synapses are common between inhibitory neurons in the mammalian thalamus and neocortex. Synaptic modulation, which allows flexibility of communication between neurons, has been studied extensively at chemical synapses, but modulation of electrical synapses in the mammalian brain has barely been examined. We found that the activation of metabotropic glutamate receptors, via endogenous neurotransmitter or by agonist, causes long-term reduction of electrical synapse strength between the inhibitory neurons of the rat thalamic reticular nucleus.

Connexin36 (Cx36)-containing gap junctions are a major mechanism of communication between the inhibitory neurons of the rodent thalamic reticular nucleus (TRN) (*1*, *2*). More than 50% of neighboring TRN neurons interact via electrical coupling. TRN neurons, which provide feedback inhibition to the thalamus, also receive strong glutamatergic synaptic inputs from neurons in the deep layers of neocortex (*3*). These corticothalamic fibers can activate metabotropic glutamate receptors (mGluRs) on TRN neurons (*2*, *4*–*7*).

We used dual whole-cell recordings in rat thalamocortical slices under infrared–differential interference contrast (IR-DIC) visualization (Fig. 1A) to measure the strength of electrical synapses interconnecting adjacent neuron pairs [coupling coefficient (cc) = 0.08 ± 0.06, mean ± SE, n = 30 pairs]. The strength of electrical coupling was tested before and after briefly tetanizing corticothalamic (CT) fibers or applying the mGluR agonist (1S,3R)-1-aminocyclopentane-1,3-dicarboxylic

[1]Department of Neuroscience, Division of Biology and Medicine, Brown University, Providence, RI 02912, USA. [2]Department of Neurobiology, Harvard Medical School, 220 Longwood Avenue, GB2-504, Boston, MA 02115, USA.

*To whom correspondence should be addressed. E-mail: Carole_Landisman@hms.harvard.edu

acid (ACPD). Ionotropic glutamatergic responses were blocked pharmacologically in all experiments.

The tetani depolarized 15 of 18 neurons tested (from nine paired recordings) (Fig. 1B); of these, 11 fired action potentials, and the remaining 3 neurons hyperpolarized in response to the stimuli. All cells recovered their baseline resting potential (V_{rest}) within 500 ms to 2 s poststimulus. Changes of coupling strength were tested after baseline recovery.

Tetanic stimulation caused a long-lasting reduction in electrical coupling strength. In one example, the coupling coefficient was reduced by 36% after the tetanus and showed no signs of recovery, even 40 min posttetanus (Fig. 1C). More detailed analysis of the time course of coupling before and after the tetanus revealed that prestimulus coupling strength varied little, but within 5 min after CT shocks the coupling coefficient dropped to steady state values, where it remained for the duration of most recordings (Fig. 1D). Both the pretetanus stability and the long-term changes in coupling strength after stimulation were found for all pairs tested (n = 9). However, two of the nine pairs showed slight recovery of coupling strength ≥ 30 min poststimulus, and one pair showed full recovery at 20 min. Overall, the coupling coefficient (cc) and the junctional conductance (Gc) (*8*, *9*) of the electrical synapses dropped for all 9 pairs (cc mean = –24% and range from –6 to –52%; Gc mean = –19% and range from –9 to –36%) (Fig. 1E). A small consistent drop caused the difference in Gc versus cc reduction in input resistance (R_{in}) after tetanic stimulation (12 of 18 cells from nine pairs), but this change was not significant (mean ± SE change = –7 ± 6%, n = 18 cells, P = 0.27, two-tailed paired t test). The tetanus-induced changes in coupling strength were prevented by including an mGluR antagonist in the bath before stimulation (Fig. 1F).

We have previously shown that TRN responses to tetanic stimulation can be simulated by application of ACPD (*2*) (fig. S1). The mGluR agonist depolarized all cells and induced continuous spiking (Fig. 2A). Three to five min after washout, resting membrane potential returned to baseline levels. Over a population of cells, there was no consistent increase or decrease in R_{in}; however, most cells did exhibit immediate changes in R_{in} (both increases and decreases) with ACPD in the bath (mean change ≤ 5 min of ACPD start = 0 ± 15%, n = 9 cells). R_{in} remained stable and similar to predrug amounts for at least 10 to 30 min post-ACPD (mean change of –7 ± 17%, P = 0.11, two-tailed paired t test). During control recordings of similar duration but without ACPD application, membrane R_{in} was stable.

ACPD reduced electrical coupling responses of TRN cells (Fig. 2B) to a degree comparable to the effects of CT tetanus. During a current step applied to TRN 1, the amplitude of the postsynaptic voltage in TRN 2 dropped 23% after ACPD application, indicating a reduction in coupling strength. The weakened response persisted after washout. All neuron pairs tested showed a decrease in coupling coefficient and coupling conductance after ACPD application [cc = –26 ± 5% and Gc = –23 ± 3% (mean reduction ± SE), n = 7 pairs) (Fig. 2E). The pooled data were similar to the single case shown (Fig. 2C) and demonstrated that 25 min of washout did not restore predrug coupling strength (Fig. 2E). As seen with the tetanus paradigm, prior application of (S)-α-methyl-4-carboxyphenylglycine (MCPG) prevented ACPD-induced changes for all pairs tested, indicating that the change in coupling strength required mGluR activation (Fig. 2, D and F).

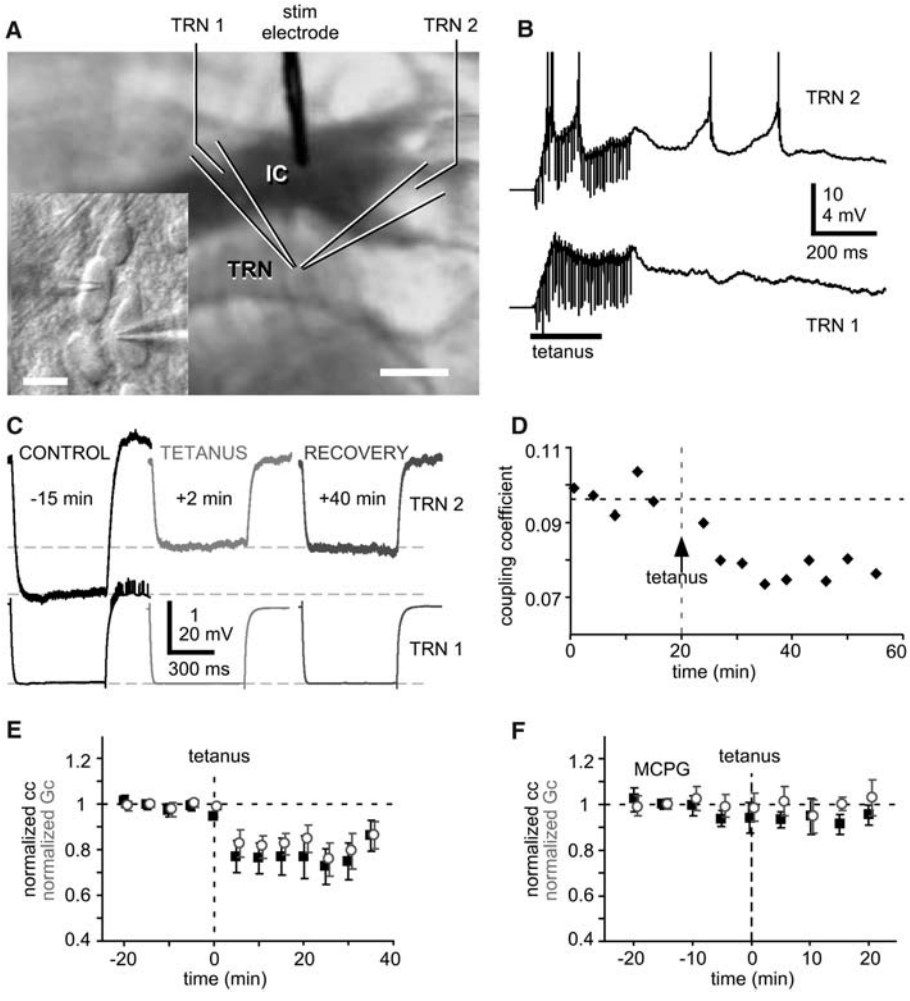

Fig. 1. Effects of tetanic stimulation on gap junction strength. (**A**) IR-DIC image of the thalamocortical slice with diagram of tetanus paradigm. Scale bars indicate 1 mm and 20 μm (inset). (Inset) High-magnification view of recorded neurons in TRN. (**B**) Responses of an electrically coupled neuron pair to tetanic stimulation. (**C**) Injected cell responses (TRN 1) and electrical coupling responses (TRN 2) before tetanus, after tetanus, and after recovery. Control cc equaled 0.11 and 0.07 immediately posttetanus to the end of recording. (**D**) Time-course measure of coupling coefficient in a pair of neurons before and after tetanus. (**E**) Normalized cc (black squares) and Gc (gray open circles) for nine pairs of cells before and after tetanic stimulation. *Y* values are normalized to the average of values collected before stimulation for each pair. (**F**) Normalized cc and Gc for four pairs before and after tetanic stimulation in the presence of MCPG. Time points represent 5-min bins, with 0 min equal to the time of tetanic stimulation. Each trace (C) and value per pair (D to F) is the average of 10 to 30 trials (mean ± SE).

We also tested the effects of modulating electrical synapses on electrical postsynaptic potentials (ePSPs) evoked by presynaptic spike bursts and by single spikes (burstlets and spikelets, respectively). ACPD consistently reduced the amplitude of both burstlets and spikelets (Fig. 3, A to D, and table S1) as well as their relative coupling strength (Fig. 3, E and F). The coupling strength of bursts and spikes were reduced by similar amounts [burst cc = –28.2 ± 7.1% and spike cc = –26.5 ± 9.9% (mean reduction ± SE), P = 0.58, two-tailed unpaired t test] (Fig. 3, E and F).

As described previously (*1*, *2*), electrical synapses between thalamic reticular neurons attenuate single spikes much more than bursts because of the low-pass filtering characteristics

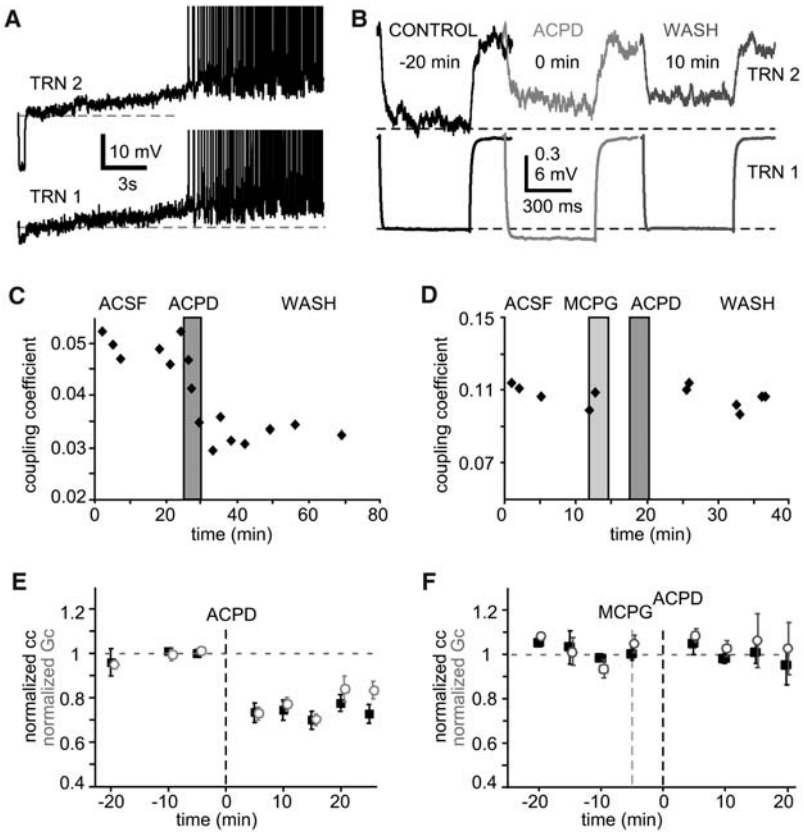

Fig. 2. Effects of ACPD on gap junction strength. (**A**) Cells depolarized to spiking during washing. A hyperpolarizing current step was delivered to TRN 1 (at trace start). (**B**) Step (–100 pA) responses (TRN 1) before, during, and after ACPD and corresponding gap junction responses (TRN 2). Control cc was 0.05 then 0.03 immediately post-tetanus through recovery. (**C**) cc time course of a neuron pair before and after ACPD application. (**D**) cc time course of a neuron pair before and after MCPG then ACPD application. Traces and time points show 10 to 30 trial averages (B to D). (**E**) cc and Gc time course for seven TRN pairs before and after ACPD application. (**F**) cc and Gc time course for five TRN pairs before drug application and after MCPG then ACPD wash. (E and F) *y* values normalized and *x* values binned as in Fig. 1F; each value per pair is the average of 10 to 30 trials. Gray bars (C and D) and dotted lines (E and F) indicate wash times. Error bars in (E) and (F) indicate SE.

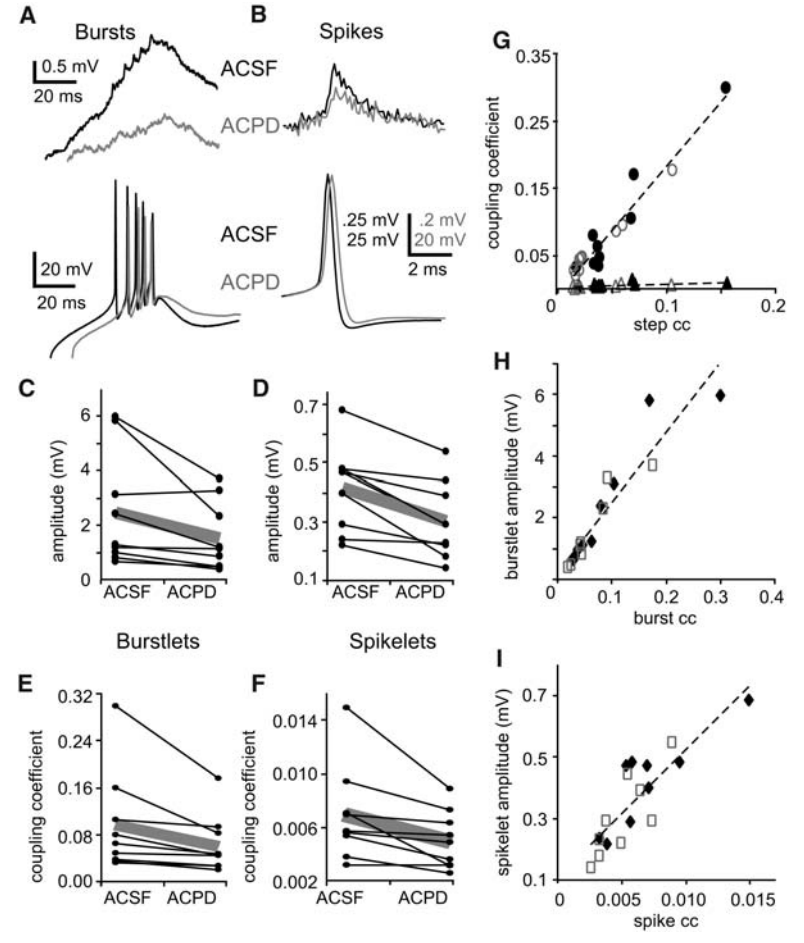

Fig. 3. Effect of ACPD modulation on gap junction transmission of spikes and bursts. (**A**) Control (black) and post-ACPD (gray) single bursts (bottom); postsynaptic burstlet responses directly above corresponding bursts. (**B**) Control (black) and post-ACPD (gray) single-action potentials (bottom) in ACSF (black) and post-ACPD (gray); spikelet responses above. (**C**) Paired average burstlet amplitudes before and after ACPD. (**D**) Paired average spikelet amplitudes before and after ACPD. (**E**) Paired average burst-to-burstlet cc before and after ACPD. Burst cc, pre- versus post-, $P < 0.04$. (**F**) Paired average spike-to-spikelet coupling coefficients before and after ACPD. Spike cc, pre- versus post-, $P < 0.03$. Two-tailed paired *t* tests (E and F). $N = 9$ cell pairs (C to F). Thick gray lines indicate population means (C to F). (**G**) The scaling relationship of direct current coupling coefficients versus burst and spike cc. Black solid symbols, control; gray open symbols, post-ACPD from the same neuron pairs; circles, burst cc; triangles, spike cc. Regression lines generated from ACSF and post-ACPD pooled data. Burstlet slope = 1.9 ($r^2 = 0.94$); spikelet slope = 0.05 ($r^2 = 0.41$). (**H** and **I**) Coupling strength versus amplitude of the postsynaptic event before and after ACPD. (H) Burstlets, slope = 23 ($r^2 = 0.87$). (I) Spikelets, slope = 42 ($r^2 = 0.73$). Burstlet data points are an average of two to four events per cell. Spikelet data points are the average of 10 to 20 events (C to I).

of the interconnected neurons and the slow voltage trajectory of a burst. On average, spike bursts evoke ePSPs with peak amplitudes about seven times larger than those of the ePSPs evoked by single spikes (table S1) [burstlet/spikelet amplitudes were 7.4 and 7.1 in artificial cerebro-spinal fluid (ACSF) and ACPD, respectively], even though the amplitudes of presynaptic spikes are about twice as large as the slow depolarizing envelope of bursts (table S1) (spike/burst amplitudes were 2.0 and 1.9 for ACSF and ACPD, respectively). The relative attenuation of bursts versus spikes is illustrated by the difference in the slopes (Fig. 3G) (*2*). Because ACPD caused very few persistent changes in the passive nonjunctional membrane properties of the neurons (table S1), there are no changes in these linear relationships of step attenuation versus burst and spike attenuation after ACPD. Additionally, the scaling factors for coupling strength versus amplitude of the postsynaptic events remained constant for burst and spike transmission (Fig. 3, H and I). The only persistent change that we observed was that most cells lost one spike per burst after ACPD application (n = 8 of 11 cells, range of 3 to 8 spikes per burst before ACPD and 2 to 7 after) (table S1).

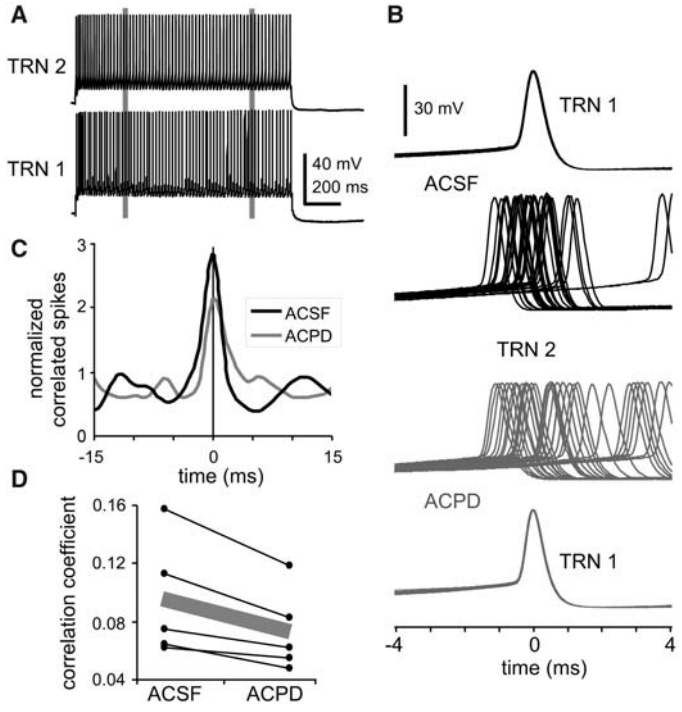

Fig. 4. Effect of reduced coupling strength on spike coordination. (**A**) Example responses of simultaneous spiking used to measure spike correlation before and after ACPD. Gray lines indicate correlation analysis window. (**B**) Demonstration of spike-triggered spikes in one trial before ACPD and one trial after for a TRN pair. The best single trial for each test was selected for comparison. Gray traces, post-ACPD, and black traces, controls (in ACSF). Top and bottom traces (TRN 1 trigger spikes) are the superimposed single spikes locked to their peaks (appear as one trace but have 40 spikes each). The middle traces (TRN 2 response spikes) are the spikes closest in time to each of the trigger spikes over an 8-ms window (±4 ms). (**C**) Cross-correlation of tonic action potentials before (black) and after (gray) ACPD for one TRN. *Y* axis normalized to average spikes per bin. Correlograms calculated from 10 consecutive trials each. (**D**) Paired correlation coefficients before and after ACPD (n = 5 cell pairs). Thick gray line is the population mean.

Presumably, one of the most important functions of gap junctions in the brain is to correlate the activity of coupled neurons (*10*–*13*). Electrical synapses of TRN cells can robustly synchronize the firing of neuron pairs under normal conditions (*1*, *2*). Thus, the reduction of coupling strength by mGluR activation could have important functional consequences for spike synchrony. We measured the effective coupling of pairs of neurons before and after ACPD and tested the strength of spike timing correlations during repetitive firing (Fig. 4). Weakening of synchrony is apparent in the single-trial example (Fig. 4B): Much larger jitter in spike timing of TRN2 relative to TRN1 is seen after ACPD treatment. Reduction of coordinated activity was also demonstrated by measuring cross-correlations of multiple trials (Fig. 4C). ACPD-induced reduction of electrical synapse strength was always accompanied by a decrease in spike synchrony, indicated by the correlation coefficients derived from cross-correlation analysis (Fig. 4D) (n = 5 pairs, P = 0.02, two-tailed paired t test).

mGluR activation (by endogenous glutamate or bath-applied agonist) caused a long-lasting, 20 to 30% reduction of electrical synapse strength between TRN neurons. The reduction of gap junction communication caused a consistent decrease in the size of both slow and fast postsynaptic events and weakened electrical synapse-mediated synchrony of spiking between pairs of TRN neurons.

Modulation of synapses by transmitters or activity has been studied extensively at mammalian chemical synapses. Modifiable strength expands the computational abilities of each synaptic contact. Activity-dependent modulation of neuronal electrical junctions, however, has not been previously characterized in the mammalian central nervous system (CNS).

Prior studies have shown gap junction modulation in other systems. Functional electrical synapses between TRN neurons require Cx36 (*1*, *11*, *13*). Cx35, the fish ortholog of Cx36, shares consensus phosphorylation sites with Cx36 (*14*). Cyclic adenosine monophosphate (cAMP) analogs cause a reduction in perch Cx35 hemichannel currents expressed in oocytes, presumably via a specific phosphorylation site (*14*). In synapses onto Mauthner cells, neural activity and activation of protein kinase II induce long-term changes of both chemical and electrical communication strength (*15*–*18*). The best evidence for modulation of Cx36 gap junctions comes from studies of retinal neurons (*19*). Mammalian amacrine cells have Cx36 gap junctions (*20*) that can be weakened by dopamine (*21*). There have also been suggestions of gap junctional modulation from tracer-coupling experiments done in neocortex (*22*), hypothalamus (*23*), and striatum (*24*) (although the relationship of these measurements to electrical coupling is unclear).

The gap junction modulation we describe here is functionally similar to mGluR-induced long-term depression at chemical synapses. In both cases, activation of mGluRs (by tetanus or agonist) induces slow postsynaptic effects lasting hundreds of milliseconds (Fig. 1B), and neuronal communication is then reduced by 20 to 50% for tens of minutes (*25*–*26*). Considering the similarities to chemical synapse modulation along with the bidirectional modulation seen at invertebrate electrical synapses, it is likely that electrical long-term potentiation (LTP) also exists at mammalian gap junction synapses (*15*–*17*).

The corticothalamic fibers originating from the deep layers of neocortex activate ionotropic AMPA, *N*-methyl-D-aspartate (NMDA), and mGluRs in cells of the mammalian dorsal thalamus (*4*–*7*). The excitatory action of the corticothalamic pathway plays a part in regulating the flow of information from sensory input, through relay nuclei of the thalamus, and into neocortex. Because mGluR activation reduces junctional coupling between TRN neurons, corticofugal input could effectively desynchronize inhibition of moderately coupled neurons that would otherwise be coordinated via electrical coupling. This decrease of coordinated inhibitory output from TRN could, in turn, enhance the efficacy of small amplitude excitatory events received by thalamic relay cells, making small sensory stimuli more salient during alert, exploratory states.

Another important role of TRN inhibition is to change the gating of thalamic relay cells from bursting to tonic mode, which is associated with changes from sleep to wakefulness (*27*, *28*). Reduced coupling strength between TRN cells during mGluR activation may contribute to the transition from thalamocortical

rhythms and burst firing to tonic firing of both TRN and relay cells (*29*). Thus, mGluRs may play a role in regulating the spatial and temporal coordination of inhibition to the dorsal thalamus.

References and Notes

1. C. E. Landisman *et al.*, *J. Neurosci.* **22**, 1002 (2002).
2. M. A. Long, C. E. Landisman, B. W. Connors, *J. Neurosci.* **24**, 341 (2004).
3. S. M. Sherman, C. Koch, *Exp. Brain Res.* **63**, 1 (1986).
4. D. A. McCormick, M. von Krosigk, *Proc. Natl. Acad. Sci. U.S.A.* **89**, 2774 (1992).
5. S. A. Eaton, T. E. Salt, *Neuroscience* **73**, 1 (1996).
6. P. Golshani, R. A. Warren, E. G. Jones, *J. Neurophysiol.* **80**, 143 (1998).
7. M. von Krosigk, J. E. Monckton, P. B. Reiner, D. A. McCormick, *Neuroscience* **91**, 7 (1999).
8. M. V. Bennett, *Ann. N. Y. Acad. Sci.* **137**, 509 (1966).
9. Y. Amitai *et al.*, *J. Neurosci.* **22**, 4142 (2002).
10. M. Galarreta, S. Hestrin, *Nat. Rev. Neurosci.* **2**, 425 (2001).
11. B. W. Connors, M. A. Long, *Annu. Rev. Neurosci.* **27**, 393 (2004).
12. M. V. L. Bennett, R. S. Zukin, *Neuron* **41**, 495 (2004).
13. S. J. Cruikshank, C. E. Landisman, J. G. Mancilla, B. W. Connors, *Prog. Brain Res.* **149**, 41 (2005).
14. G. Mitropoulou, R. Bruzzone, *J. Neurosci. Res.* **72**, 147 (2003).
15. X. D. Yang, H. Korn, D. S. Faber, *Nature* **348**, 542 (1990).
16. A. E. Pereda, A. Triller, H. Korn, D. S. Faber, *Proc. Natl. Acad. Sci. U.S.A.* **89**, 12088 (1992).
17. A. Pereda *et al.*, *Proc. Natl. Acad. Sci. U.S.A.* **95**, 13272 (1998).
18. M. Smith, A. E. Pereda, *Proc. Natl. Acad. Sci. U.S.A.* **100**, 4849 (2003).
19. E. M. Lasater, J. E. Dowling, *Proc. Natl. Acad. Sci. U.S.A.* **82**, 3025 (1985).
20. M. R. Deans, B. Volgyi, D. A. Goodenough, S. A. Bloomfield, D. L. Paul, *Neuron* **36**, 703 (2002).
21. E. C. Hampson, D. I. Vaney, R. Weiler, *J. Neurosci.* **12**, 4911 (1992).
22. B. Rörig, G. Klausa, B. Sutor, *J. Neurosci.* **15**, 7386 (1995).
23. P. Cobbett, G. I. Hatton, *J. Neurosci.* **4**, 3034 (1984).
24. P. O'Donnell, A. A. Grace, *J. Neurosci.* **13**, 3456 (1993).
25. X. D. Yang, J. A. Connor, D. S. Faber, *J. Neurophysiol.* **71**, 1586 (1994).
26. S. H. Oliet, R. C. Malenka, R. A. Nicoll, *Neuron* **18**, 969 (1997).
27. M. Steriade, L. Domich, G. Oakson, *J. Neurosci.* **6**, 68 (1986).
28. M. Steriade, D. A. McCormick, T. J. Sejnowski, *Science* **262**, 679 (1993).
29. K. H. Lee, D. A. McCormick, *Neuroscience* **77**, 335 (1997).

30. All animal procedures were reviewed and approved by Brown University, in accordance with NIH guidelines. We thank J. Gibson for writing software, S. Patrick for technical assistance, and S. Cruikshank for helpful suggestions. Supported by NIH grants NS40528, NS25983, and NS050434 and Shore Scholars in Medicine Program, Harvard Medical School (C.E.L.).

Supporting Online Material

www.sciencemag.org/cgi/content/full/310/5755/1809/DC1
Materials and Methods
Fig. S1
Table S1

10 May 2005; accepted 11 November 2005
10.1126/science.1114655

Glial Membranes at the Node of Ranvier Prevent Neurite Outgrowth

Jeffrey K. Huang,[1,2] Greg R. Phillips,[1] Alejandro D. Roth,[3] Liliana Pedraza,[3] Weisong Shan,[3] Wiam Belkaid,[3] Sha Mi,[4] Asa Fex-Svenningsen,[5] Laurence Florens,[6] John R. Yates III,[7] David R. Colman[1,3]*

Nodes of Ranvier are regularly placed, nonmyelinated axon segments along myelinated nerves. Here we show that nodal membranes isolated from the central nervous system (CNS) of mammals restricted neurite outgrowth of cultured neurons. Proteomic analysis of these membranes revealed several inhibitors of neurite outgrowth, including the oligodendrocyte myelin glycoprotein (OMgp). In rat spinal cord, OMgp was not localized to compact myelin, as previously thought, but to oligodendroglia-like cells, whose processes converge to form a ring that completely encircles the nodes. In OMgp-null mice, CNS nodes were abnormally wide and collateral sprouting was observed. Nodal ensheathment in the CNS may stabilize the node and prevent axonal sprouting.

Myelin sheaths that wrap around neuronal axons are periodically interrupted by nodes of Ranvier that enable saltatory conduction (*1*) (Fig. 1A). After peripheral nervous system (PNS) injury, axonal sprouting from neighboring unlesioned nerves commonly occurs at nodes of Ranvier, allowing for the reestablishment of functional neurocircuitry (*2*, *3*). In contrast, injury-induced sprouting rarely occurs at CNS nodes despite the absence of myelin, which is inhibitory to neurite outgrowth (*4*). One explanation for the nonresponsiveness of CNS axons to injury might be that sprouting is prevented by nonmyelin-derived factors present in the nodal vicinity.

To identify such inhibitory factors, we isolated membranes of the mammalian CNS nodal axoglial apparatus, comprising the node and flanking paranodal domains, by subcellular fractionation of dissected bovine, mouse, or human white matter. Because the nodal axoglial apparatus is morphologically distinct from myelin (Fig. 1B) and likely to be of greater density due to a higher protein:lipid ratio than myelin, we reasoned that membranes of the nodal axoglial apparatus might be sheared away during homogenization and be concentrated at an isopycnic density greater than that of compact myelin. We modified a synaptosome protocol (*5*) by using as starting material CNS white matter that contained myelinated axons and was devoid of synaptic endings. Membrane fractions were recovered from sucrose density gradients at a 0.32/1.0 M interface, comprising compact myelin membranes (*6*), and at a 1.0/1.25 M interface, which we provisionally termed "axogliasomes." Ultrastructural examination of axogliasomes revealed membrane profiles characteristic of paranodal loops, attached to underlying axolemmal fragments (Fig. 1C). In contrast, profiles of compact myelin and synaptosomes were rarely detected. Immunoelectron microscopy examination with a paranode-specific marker, Caspr (*7*, *8*), confirmed that the observed membranes were derived from the nodal axoglial apparatus (Fig. 1D). We also investigated whether axogliasomes contained appropriate biochemical markers for the nodal axoglial apparatus. The known paranodal markers Caspr, contactin, and neurofascin-155 (*9*), as well as the nodal marker, neurofascin-186 (*10*), were all detected by Western blot analysis of the axogliasome fraction, whereas compact myelin-specific markers, the proteolipid proteins PLP and DM20, were barely detected (Fig. 1E). The detection of myelin-associated glycoprotein (MAG) in compact myelin and axogliasomes was expected, because it is expressed throughout periaxolemmal channels of compact myelin and at paranodes (*11*). Axogliasomes are thus morphologically and biochemically distinct from membranes derived from compact myelin and comprise the entire nodal axoglial apparatus.

It is well established that purified compact myelin membranes can effectively limit neurite outgrowth activity in cell culture owing to myelin-specific inhibitory factors (*4*). To determine if CNS nodes of Ranvier also contain inhibitory factors for axon outgrowth,

[1]Fishberg Department of Neuroscience, Mount Sinai School of Medicine, One Gustave L. Levy Place, New York, NY 10029, USA. [2]Wellcome Trust/Cancer Research UK Gurdon Institute, University of Cambridge, Tennis Court Road, Cambridge CB2 1QR, UK. [3]The Montreal Neurological Institute, McGill University, 3801 University Street, Montreal PQ H3A 2B4, Canada. [4]Biogen Idec, Discovery Biology, 14 Cambridge Center, Cambridge, MA 02142, USA. [5]Department of Genetics and Pathology, Rudbeck Laboratory, Uppsala University, SE-751 85 Uppsala, Sweden. [6]Stowers Institute, 1000 East 50th Street, Kansas City, MO 64110, USA. [7]Department of Cell Biology SR11, The Scripps Research Institute, 10550 North Torrey Pines Road, La Jolla, CA 92037, USA.

*To whom correspondence should be addressed. E-mail: david.colman@mcgill.ca

Long-Term Modulation of Electrical Synapses in the Mammalian Thalamus

Carole E. Landisman and Barry W. Connors

Science **310**, 1809 (2005);
DOI: 10.1126/science.1114655